J. Wind Eng. Ind. Aerodyn. 115 (2013) 53–64

Contents lists available at SciVerse ScienceDirect

Journal of Wind Engineering and Industrial Aerodynamics

journal homepage: www.elsevier.com/locate/jweia

# An analytical model for simulating steady state flows of downburst

El-Sayed Abd-Elaal, Julie E. Mills *, Xing Ma

*School of Natural and Built Environments, University of South Australia, Mawson Lakes, SA 5095, Australia*

ARTICLE INFO

*Article history:*
Received 15 June 2012
Received in revised form
23 January 2013
Accepted 26 January 2013
Available online 26 February 2013

*Keywords:*
Downburst
Analytical model
Shaping functions
Boundary layer

ABSTRACT

Downburst wind events represent the greatest threat to many structural engineering systems due to the extreme wind that they generate. They have been shown to be the cause of many past failures of many structural systems. There are many experimental and numerical models for simulating these types of loads. However, analytical and empirical simulation models are needed to facilitate the analysis of structural systems under these types of loads. There are remarkable disparities between the available analytical models and the recorded field data, experimental and numerical simulations. Added to that, the effects of nonlinear growth of boundary layer thickness are rarely included in these models. This paper presents an analytical model that successfully matches the recorded field data, experimental and numerical results. Two new empirical functions which are able to simulate the radial and vertical profiles of horizontal downburst wind speed have been developed. These two equations have then been implemented into the continuity equation and the vertical and radial profiles of the vertical downburst wind speed have been estimated analytically. Once boundary layer effects have been included in the model, the radius corresponding to maximum wind speed becomes a function of elevation, the height corresponding to maximum wind speed becomes a function of the radial coordinates and the shapes of the speed profiles become changeable with the radial and vertical coordinates.



## 1. Introduction

Wind loads represent the prevalent critical loads for many structural systems such as transmission towers. Dempsey and White (1996) recorded that more than 80% of all failures of transmission towers around the world result from high intensity winds, ranging from the different forms of microburst and downbursts to fully mature tornadoes. For example, the failure of 19 transmission towers was reported during a microburst event in Manitoba, Canada in 1996 (McCarthy and Melsness, 1996). Similarly, Li (2000) reported that more than 90% of transmission tower failures in Australia are due to severe thunderstorms involving downburst events and Zhang (2006) recorded the failure of 75 transmission towers due to the strong wind events such as downburst and tornadoes in China in 2005.

The formation and extension of downburst winds are different from those of boundary layer winds. Downbursts occur when warm air rises and ascends above the cloud, creating a dome of warm air. The air cools at this height and then begins to fall, collapsing the dome and rushing back to the ground, forming an outburst of damaging air ('Downbursts' of air are called danger to aircraft, 1979).

Downburst wind speed and the associated loads acting on structural systems vary with downburst parameters such as downburst width, coordinates of the centre of the downburst relative to the centre of the structural system, downflow velocity and so on. In addition, each element in the structural system has different downburst parameters that produce maximum internal forces in those elements (Shehata et al., 2008). Investigation of structural systems under downburst loads is so complex that analytical and empirical models for simulating these types of loads are necessary to facilitate the analysis and design of structural systems subjected to them.

Earlier researchers presented several analytical and empirical models of wind speeds for simulating downburst wind loads. Oseguera and Bowles (1988) developed the first analytical model for non-turbulent downburst wind speed. They proposed that the vertical and horizontal components of downburst wind speed could be estimated by multiplying the vertical and horizontal shaping functions for each component. They developed a pair of shaping functions that were able to simulate velocity profiles of terminal area simulation systems (TASS) (Proctor, 1987), and employed the mass continuity equation for deriving the corresponding pair of shaping functions. Vicroy (1991) studied the previous model and improved the radial shaping function of horizontal wind speed and then improved the vertical shaping function of horizontal wind speed Vicroy (1992). However, there is still a significant difference between these models and the available field and numerical data.

* Corresponding author. Tel.: +61 883023073.
*E-mail address:* julie.mills@unisa.edu.au (J.E. Mills).

0167-6105/$ - see front matter © 2013 Elsevier Ltd. All rights reserved.
http://dx.doi.org/10.1016/j.jweia.2013.01.005

**Nomenclature**

$D$ diameter of downburst (m)
$f(r)\{p(z)\}$ radial {vertical} shaping function of the horizontal wind speed
$f_m(r)\{p_m z\}$ radial {vertical} shaping function of the maximum horizontal wind speed
$g(r^2)\{q(z)\}$ radial {vertical} shaping function of the vertical wind speed
$R_c$ characteristic length scale in Holmes' and Li et al.'s models
$r,\phi,z$ cylindrical coordinates
$r_m$ radius at the overall maximum horizontal speed (m)
$u\{w\}$ wind speed in the radial {vertical} direction (m/s)
$u_{\max}$ magnitude of overall maximum horizontal speed (m/s)
$u_{m,rs}(r)\{u_{m,vs}(z)\}$ radial {vertical} shaping function of the maximum horizontal wind speed in Li et al.'s models
$w_{jet}$ jet speed (m/s)
$w_{\max}$ magnitude of maximum vertical speed (m/s)
$w_0$ vertical speed at the centre of downburst (m/s)
$w_{0m}$ vertical speed at the centre of downburst at altitude of peak horizontal speed (m/s)
$z_h$ depth of outflow (m)
$z_m$ height at the overall maximum horizontal speed (m)
$z^*$ altitude at which the magnitude of horizontal speed is half the peak speed (m/s)
$v$ tangential speed in radial coordinate (m/s)
$\xi_1,\xi_2,c_1,c_2,\gamma,\beta,\delta,\varepsilon,\kappa,\chi,A,B,C,\eta,\iota,\varphi$ non dimensional parameters
$\lambda$ scaling factor ($s^{-1}$)

Holmes and Oliver (2000) presented an empirical function for simulating the radial profile of horizontal wind speed at 10 m height. Their function is more accurate in depicting the profile of downburst wind speed, but it is limited to the radial profile of horizontal wind speed. Wood et al. (2001) introduced an empirical function for simulating the vertical distribution of horizontal wind speed. Sengupta and Sarkar (2008) improved Wood et al.'s (2001) function by enhancing its parameters. The two empirical functions of Holmes and Oliver (2000) and Wood et al. (2001) matched the available field and numerical data, but they are limited to the horizontal downburst wind speed.

Chay et al. (2006a) improved the previous analytical model of Oseguera and Bowles (1988) and Vicroy (1991) by introducing several modifications to the model parameters. They also recommended adding the boundary layer effects through developing the height corresponding to maximum wind speed to become a function of distance from downburst centre. Again, Chay et al. (2006b) developed the shaping function of the vertical distribution of horizontal wind speed by replacing the radial shaping functions of the horizontal velocity by Wood et al.'s (2001) function. But they did not consider the continuity equation which controls the relation between the vertical and the horizontal speed.

Li et al. (2012) upgraded the earlier Oseguera and Bowles (1988) and Vicroy (1991) model by implementing the previous two empirical equations of Holmes and Oliver (2000) and Wood et al. (2001) to the continuity equation and then developed the corresponding equations for the vertical wind speed. However, the developed formula for vertical wind speed cannot be expressed in terms of elementary functions and so is complex to use. They inserted the nonlinear effects of boundary layer growth to the model by improving two empirical equations that are able to depict the variations in the horizontal and vertical coordinate of maximum horizontal wind speed. Their model was able to depict the profiles of horizontal wind speed including nonlinear effects of boundary layer growth, but failed to depict the variation of profiles of vertical wind speed and did not satisfy the continuity equation which confirms the relationship between the vertical and the horizontal downburst wind speed.

This study provides answers for the issues in the previous models by introducing a new pair of shaping functions that are able to simulate profiles of downburst wind speed and match the available field and numerical data with high accuracy. The vertical and radial profiles of vertical wind speeds have been estimated by using Euler and mass continuity equations and the new functions are characterized by their simplicity and simple integration. The nonlinear effects of boundary layer growth on the coordinates of the maximum wind speed have been included without dropping the continuity equation, and the changes in the shapes of the profiles due to the boundary layer effects have been introduced.

## 2. Model development

Oseguera and Bowles (1988) and Vicroy (1991) developed an analytical model for simulating downburst wind loads by solving the mass continuity equation and assuming a pair of shaping functions which were able to simulate velocity profiles at the altitude and the radial position of the maximum speed (Proctor, 1987). Their model has been summarised in the Appendix. In this study, their previous model will be derived again but the selected shaping function for the vertical and radial profile of the horizontal wind speed will be improved.

### 2.1. Shaping function for the vertical profile of the horizontal wind

The shaping function for the vertical profile of the horizontal wind speed for the models of Oseguera and Bowles (1988), and Vicroy (1992) has a remarkable difference with radar observation by Hjelmfelt (1988) and the recent experimental and numerical simulation results for downburst wind by Wood et al. (2001), Kim and Hangan (2007), Sengupta and Sarkar (2008) and McConville et al. (2009). Wood et al. (2001) developed the following empirical equation which matches their numerical and experimental results:

$$u(z) = A\left(\frac{z}{z^*}\right)^B \left[1-\mathrm{erf}\left(C\frac{z}{z^*}\right)\right] \quad (1)$$

where erf is the error function, the parameters $A$, $B$ and $C$ are 1.55, 1/6 and 0.7, respectively and $z^*$ is defined as the altitude at which the magnitude of horizontal speed is half the maximum speed. The elevation $z^*$ can be expressed in terms of $z_m$ where $z_m$ is the height of the maximum horizontal wind speed. It has been stated that $z^*$ is in the range of $6.0\,z_m$ (Wood et al. 2001). This model matches field, experimental and numerical data better than the Oseguera and Bowles (1988) and Vicroy (1991) models that have a significant difference between the available data, in particular, for heights less than $z_m$. Sengupta and Sarkar (2008) improved the parameters $A$, $B$ and $C$ to be 1.52, 1/6.5 and 0.68, respectively. Li et al. (2012) revised the model parameters, estimated implicit relationships between the parameters and developed a simple

function in one parameter as follows:

$$p(z) = \left(\frac{z}{z_m}\right)^{\gamma} e^{\gamma(1-z/z_m)} \tag{2}$$

There is a small disparity between Eq. (2) and the available data, but the main problem with this function and Wood et al.'s (2001) function arises during deriving of the corresponding vertical shaping function $q(z)$. Li et al. (2012) applied Eq. (2) to the continuity equation and derived the corresponding function $q(z)$, resulting in the following function:

$$q(z) = \frac{\int_0^z (z/z_m)^{\gamma} e^{\gamma(1-z/z_m)} dz}{\int_0^{\infty} (z/z_m)^{\gamma} e^{\gamma(1-z/z_m)} dz} \tag{3}$$

This function cannot be expressed in terms of elementary functions and needs a numerical integration at each height which complicates the model. In this study, a new simple equation for the vertical shaping function of the horizontal wind velocity has been presented as follows:

$$p(z) = \left(\frac{z}{z_m}\right)^{c_2-1} e^{c_1\left(\frac{z}{z_m}\right)^{c_2}} \tag{4}$$

The new function achieves greater accuracy than the previous functions. Fig. 1 shows the shape of the new function and the shapes of a selection of the previous models. The new function matches the empirical model of Sengupta and Sarkar (2008), the numerical results of Kim and Hangan (2007) and McConville et al. (2009), and the radar observation by Hjelmfelt (1988). There is a simple relationship between the parameter $c_1$ and $c_2$ which will further simplify the equation to one parameter and will be discussed in Section 3.1.

The corresponding derived function for the vertical speed profile $q(z)$ is given in Eq. (5). The new function $q(z)$ is easier to use than the previous function Eq. (3), and its profile is shown in Fig. 2, which compares well with the previous results. The vertical profiles of the horizontal and the vertical wind speeds in Fig. 1 and Fig. 2, respectively, have been normalized by $z^*$ which has been utilised in the previous numerical results. Li et al.'s (2012) model and the proposed model depends on $z_m$. Their results have been normalized by replacing the value $z^*$ by $5.9\,z_m$ and the precise relationship between $z^*$ and $z_m$ will be discussed in Section 3.1.

$$q(z) = -\lambda \frac{z_m}{c_1 c_2}\left[e^{c_1\left(\frac{z}{z_m}\right)^{c_2}} - 1\right] \tag{5}$$

### 2.2. Shaping function for radial profile of the horizontal wind

Holmes and Oliver (2000) developed an empirical model for the radial profile of horizontal wind speed as presented in Eq. (6), which agrees more closely with the field and numerical data than the Oseguera and Bowles (1988) and Vicroy (1991) model. Li et al. (2012) further developed this empirical model by enhancing the parameters $\beta$ and $R_c$ to be $\beta = 0.1287$, $R_c = 0.599 r_m$ where $r_m$ is the radius at the location of the maximum horizontal speed.

$$f(r) = \begin{cases} r/r_m & r \le r_m \\ e^{-[(r-r_m)/R_c]^{\beta}} & r > r_m \end{cases} \tag{6}$$

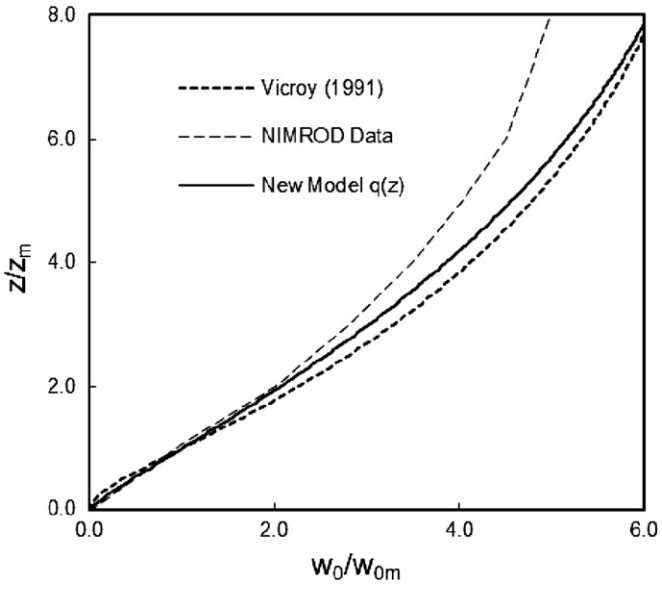


**Fig. 2.** Comparison of vertical profiles of normalized vertical winds.

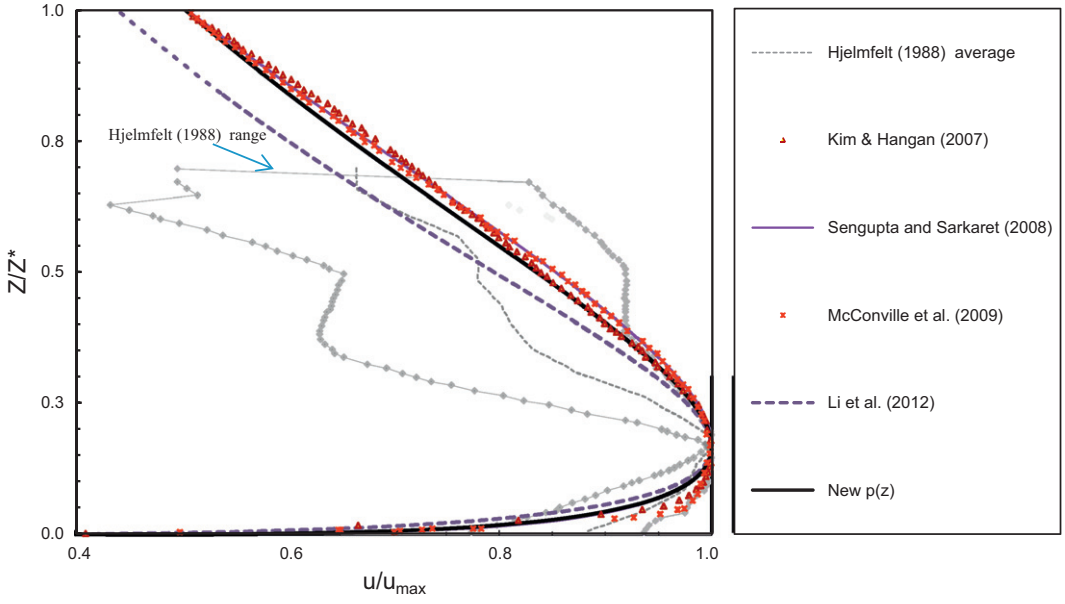


**Fig. 1.** Comparison of the vertical profiles of normalized horizontal winds.

The model consists of two different equations related to the radial distance. Li et al. (2012) applied the function $f(r)$ to the continuity equation and derived the corresponding vertical shaping function $g(r^2)$ as follows:

$$g(r^2)=\begin{cases}1 & r\le r_m\\ \frac{e^{-[(r-r_m)/R_c]^\beta}}{2r}-\frac{\beta((r-r_m)/R_c)^{\beta-1}\,e^{-[(r-r_m)/R_c]^\beta}}{2R_c} & r>r_m\end{cases} \tag{7}$$

The function $g(r^2)$gives a constant distribution in the range $r<r_m$ and this distribution does not match the available field data (Proctor, 1987) as shown in Fig. 3. In this study, a new function for the radial profile of the horizontal wind speed is presented as follows:

$$f(r)=\frac{\lambda r}{2}\left[e^{-\left[2\gamma-(\delta r^2/{r_m}^2)^\gamma\right]^2}+\varepsilon e^{-\kappa(r^2/{r_m}^2)^\chi}\right] \tag{8}$$

where $\gamma,\delta,\varepsilon,\kappa$ and $\chi$ are the shaping function variables.

Fig. 4 shows the shape of the new radial function $f(r)$ and shapes of the previous analytical models, Vicroy (1991) model, the empirical model of Holmes and Oliver (2000) and Li et al.'s (2012) model. The proposed shaping function compares well with the mean data of radar observation by Hjelmfelt (1988). It also compares well with the empirical function (Eq. (6)) proposed by Li et al. (2012) except that the proposed shaping function consists of only one part for all radial distances, which will simplify the new model. The corresponding radial shaping function $g(r^2)$ for mean vertical wind speed is:

$$g(r^2)=(1+2\gamma\psi(2\gamma-\psi))e^{-[2\gamma-\psi]^2}+\varepsilon e^{-\kappa(r^2/{r_m}^2)^\chi}\left(1-\kappa\chi\left(\frac{r^2}{{r_m}^2}\right)^\chi\right)$$

$$\text{and}\quad \psi=\left(\frac{\delta r^2}{{r_m}^2}\right)^\gamma \tag{9}$$

The new function $g(r^2)$ corresponds more closely to the (Proctor, 1987) data and the numerical results compared with the previous model as shown in Fig. 3. There are discrepancies for the $r<r_m$ range. The CFD model and the (Proctor, 1987) data predict the maximum vertical speed ($w_m$) at a smaller radial distance, however, further development to the $g(r^2)$ function will cause deviation to the profile of the $f(r)$ function, where the two functions are connected by the continuity equation. In this study the best parameters that simulate the two functions together have been applied, and the priority has been given to the $f(r)$ function, where the horizontal wind speed is the main wind component. The horizontal profiles of the vertical and the horizontal wind speeds in Figs. 3 and 4 have been normalized by $r_m$ which has been employed in the referenced results. The two functions $f(r)$ and $g(r^2)$ have been established with the feature that their profiles are a function of $(r/r_m)$ and by this approach the model will be flexible to the values of $r_m$. The locations of the maximum speed will be able to be shifted to smaller or larger radial distances according to the relationship between $r_m$ and $D$ (discussed in Section 3.2) and there are other benefits of the new proposed function that will be discussed in Section 4.4.

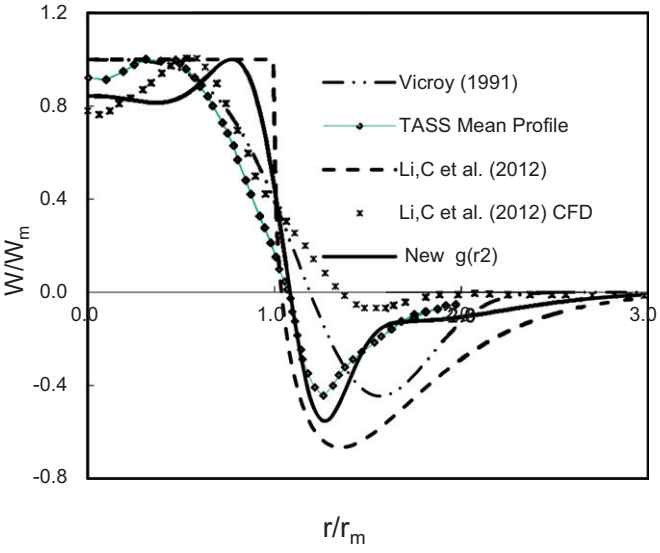


**Fig. 3.** Comparison of normalized vertical wind profiles along the radial.

## 3. Model characteristics

Bearing in mind that the horizontal component of downburst wind speed represents a more significant threat to structures than the vertical component, the proposed analytical model has been established by developing two empirical functions $p(z)$ and $f(r)$ which are able to simulate the profiles of the horizontal wind speed, while the profiles of the vertical wind speed have been derived by solving the continuity equations. The final equations for the horizontal and vertical wind speed can be computed by summating the two new functions $f(r)$ and $p(z)$ with the two derived functions $g(r^2)$ and $q(z)$ as presented in the Oseguera and Bowles (1988), and Vicroy (1991) model as follows:

$$u=\frac{\lambda r}{2}\left[e^{-[2\gamma-\psi]^2}+\varepsilon e^{-\kappa(r^2/{r_m}^2)^\chi}\right]\left[\left(\frac{z}{z_m}\right)^{c_2-1}\;e^{c_1\left(\frac{z}{z_m}\right)^{c_2}}\right] \tag{10}$$

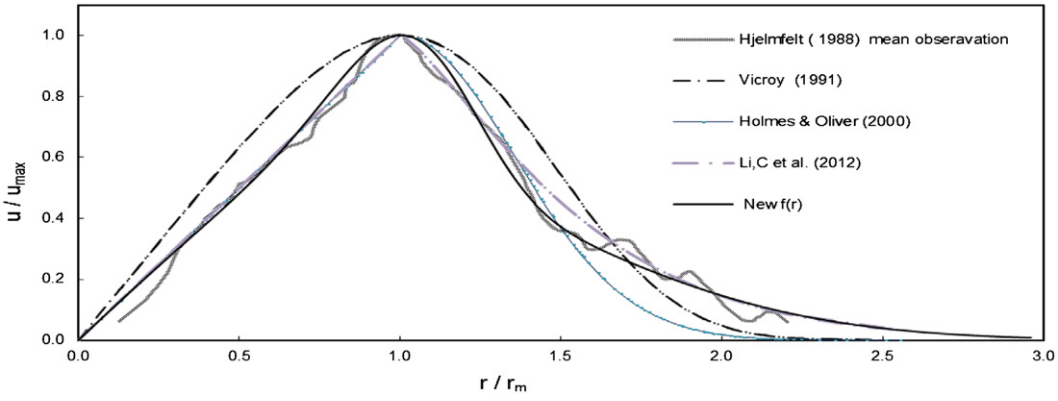


**Fig. 4.** Comparison of normalized horizontal wind profiles along the radial.

$$w=-\lambda\left\{(1+2\gamma\psi(2\gamma-\psi))e^{-[2\gamma-\psi]^2}+\varepsilon e^{-\kappa(r^2/r_m{}^2)^\chi}\left(1-\kappa\chi\left(\frac{r^2}{r_m{}^2}\right)^\chi\right)\right\}$$
$$\left\{\frac{z_m}{c_1c_2}\left[e^{c_1\left(\frac{z}{z_m}\right)^{c_2}}-1\right]\right\} \quad (11)$$

where $\psi=(\delta r^2/r_m{}^2)^\gamma$, and $u$ and $w$ are the horizontal and the vertical wind speed (m/s), respectively. By taking the derivatives of Eqs. (10) and (11) with respect to $r$ and $z$ and substituting in the continuity equations, the new model satisfies the continuity equation.

At this stage of the model development the coordinates of the maximum horizontal speed remain fixed at the location of overall maximum horizontal speed. This did not consider the changes in the location of maximum speed due to the nonlinear growth of boundary layer thickness. $r_m$ and $z_m$ are the radius and height at the location of the overall maximum horizontal speed, respectively, and their values will be discussed in the following sections.

### 3.1. Vertical profile of horizontal wind

The new shaping function for the vertical profile of the horizontal wind velocity has been established with the standard characteristic, the height of maximum horizontal speed occurs at $z_m$. For examining the height of the maximum horizontal velocity, the partial derivative of $u$ with respect to $z$ was set to equal zero, then substituting $z/z_m=1.0$ which keeps the height of maximum velocity at $z=z_m$, the following relationship between $c_1$ and $c_2$ is found.

$$c_2=\frac{1}{1+c_1} \quad (12)$$

This relationship holds the maximum velocity at $z=z_m$, and the function now becomes in one parameter $c_1$. The value of $c_1$ which reflects the shaping profile has been calculated to be $-0.133$ and the corresponding value for $c_2$ is 1.1534. The value of $z_m$ can be assumed according to the existing numerical results and field data. A review for the height of maximum horizontal velocity form several researchers is summarized in Table 1. The characteristic height $z^*$ which has been used for normalizing the elevation in Fig. 1 is indicated by (Proctor, 1987) data as $z^*=4.46\,z_m$. Oseguera and Bowles (1988) and Vicroy (1991) kept the same definition, but later Vicroy (1992) changed $z^*$ to be $6.67z_m$. Wood et al. (2001), Kim and Hangan (2007) and McConville et al. (2009) stated that $z^*=6.25z_m$ to $5.88z_m$. From this review the value of $z_m$ that has been applied in the proposed model is $0.016D$ and the corresponding value for characteristic height $z^*$ will be $5.9z_m$ according to model calculation.

### 3.2. Radial profile of horizontal wind

The radial shaping function of the horizontal wind velocity has been developed with the characteristic that, the location of maximum horizontal speed occurs at $r_m$. There are several values for the parameters $\gamma,\delta,\varepsilon,\kappa$ and $\chi$ which realize the location of maximum horizontal velocity at $r_m$, but the best values for parameters that can depict the shaping profile while holding the location of maximum at $r_m$ have been calculated to be 0.85, 2.0, 2.0, 0.6 and 1.05, respectively. For examining the radial location of the maximum horizontal velocity, the partial derivative of $u$ with respect to $r$ was set to equal zero. The resulting equation from the derivative is:

$$\left[1+4\psi\gamma(2\gamma-\psi)\right]e^{-\left[2\gamma-(\delta r^2/r_m{}^2)^\gamma\right]^2}=\varepsilon e^{-\kappa(r^2/r_m{}^2)^\chi}(2\chi\kappa)\left(\frac{r^2}{r_m{}^2}\right)^\chi \quad (13)$$

The value 1.0 was obtained from iteration for the ratio $r/r_m$ which realizes the position of maximum velocity at $r=r_m$. The position of maximum velocity $r_m$ can be assumed as a ratio of $D$. Table 2 presents a review for the radial position of maximum horizontal velocity. From this review the value for $r_m$ that has been implemented in the new model is $1.125D$.

### 3.3. Scaling factor

Using the new model, the maximum horizontal velocity can be expressed as Eq. (14) and the maximum vertical velocity at $r=0$

**Table 1**
Summary of height of maximum horizontal velocity.

| Author | Height of maximum horizontal velocity | Comments |
|---|---|---|
| Hjelmfelt (1988) | 50 to 100 m | Stated from the recorded field data. |
| Wood et al. (2001) | $0.016D$ | The height of maximum velocity increases with increasing radial distance. |
| Hangan et al. (2003) | $0.02D$ to $0.03D$ | Conducted experimental and numerical simulation |
| Chay et al. (2006a) | $0.023D$ to $0.025D$ | Indicated from computational fluid dynamics with experimental investigation |
| Kim and Hangan (2007) | less than $0.05D$ | Conducted numerical simulations of impinging jet steady state and unsteady state |
| Xu and Hangan (2008) | $0.03D$ | Stated during experimental investigation |
| Mason et al. (2009) | $0.011D$ | Conducted numerical simulation using cooling source approach, the maximum velocity occurs at relative elevation $z_m=0.011D$ and this ratio reduces with increasing downburst diameter, for $D=0.55$ km is $0.015D$, for $D=1$ km is $0.011D$, for $D=1.5$ km is $0.009D$ and for $D=2$ km is $z_m=0.007D$. |
| Vermeire et al. (2011) | $0.015D$ | Conducted numerical simulation using cooling source approach |

**Table 2**
Summary of radial position of maximum horizontal velocity.

| Author | Radial position of maximum horizontal velocity | Comments |
|---|---|---|
| Hjelmfelt (1988) | $0.75D$ to $1.0D$ | Implied from the recorded field data |
| Chay et al. (2006a) | $1.0D$ to $1.25D$ | Indicated from computational fluid dynamics with downburst wind tunnel |
| Kim and Hangan (2007) | $1.1D$ | Conducted numerical simulations of impinging jet steady state and unsteady state |
| Xu and Hangan (2008) | $1.1D$ | Conducted experimental investigation |
| Mason et al. (2009) | $1.25D$ | Conducted numerical simulation using cooling source approach |
| Vermeire et al. (2011) | $1.425D$ | Conducted numerical simulation using cooling source approach |

and $z = z_h$, is given by Eq. (15).

$$u_{max} = 0.913\lambda\, r_m \tag{14}$$

$$w_{max} = 13.4\,\lambda\, z_m\,(e^{-0.133\,(z_h/z_m)^{1.1534}} - 1) \tag{15}$$

The scaling factor $\lambda$ can be determined by using either Eq. (14) or Eq. (15) and setting it equal to $u_{max}$ or $w_{max}$, respectively. In the next sections the nonlinear effects of boundary layer thickness growth will be investigated and their effect on the wind profiles will be included.

## 4. Considering the effects of nonlinear growth of boundary layer thickness

Many researchers have studied the development of boundary layer thickness during experimental and numerical simulation of microburst and downburst (Letchford and Mans, 1999; Wood et al., 1999, 2001; Chay and Letchford, 2002; Mason, 2003; Sengupta and Sarkar, 2008; Li et al., 2012). During spreading of downburst wind, downburst wind speeds and their profiles vary with time and space. The proposed study deals with the variation in space only (steady state simulation). Figs. 5 and 6 illustrate the changes of the vertical and radial profile of the horizontal velocity with the radial and vertical coordinates, due to the nonlinear growth of boundary layer thickness. The effects of nonlinear growth of boundary layer thickness can be summarised in three primary points, the change in the height of maximum horizontal speed ($z_m$), change in the radial coordinate of maximum horizontal speed ($r_m$) and change in the shapes of the wind profiles. The first two points have been studied by several researchers and will be revised and improved, while the third point will be initiated here.

### 4.1. Height of maximum horizontal speed

The height of the maximum horizontal speed changes with traveling in the radial direction from the centre of downburst until the speed disappears. Letchford and Mans (1999), Wood et al. (1999, 2001), Chay and Letchford (2002) and Mason (2003) studied the change in the height of the maximum speed. Their studies varied between experimental and numerical simulation. A review of variations of height of maximum speed $z_m$ with radial distance has been summarized in Fig. 7. Sengupta and Sarkar (2008) and Li et al. (2012) studied the change of height of half the maximum speed $z^*$ instead of $z_m$. Li et al. (2012) stated that $z_m$ is too close to the ground and is difficult to calculate precisely. Hence they chose to use $z^*$ as a boundary layer characteristic thickness parameter.

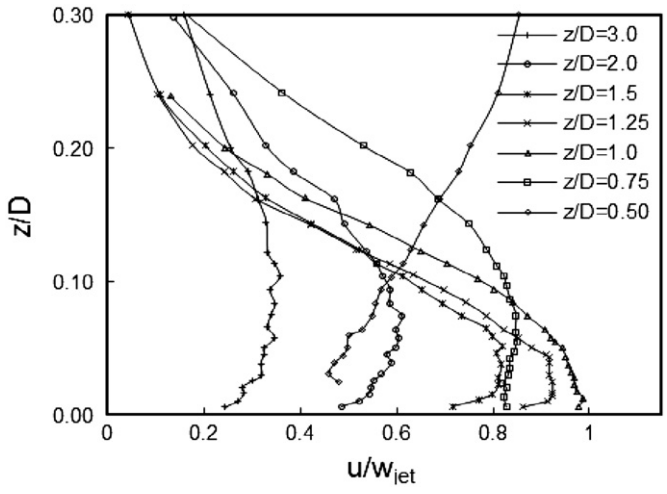


**Fig. 5.** Change of the vertical profile of horizontal speed with radial distance (Chay et al. 2006a).

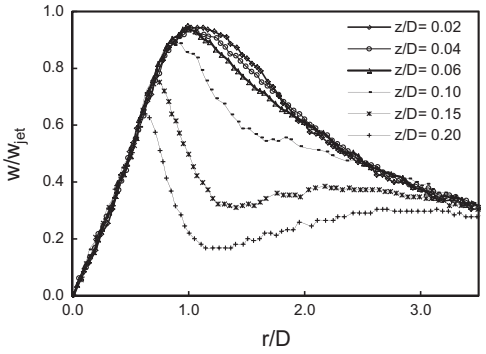


**Fig. 6.** Change of the radial profile of horizontal speed with elevation (Li et al. 2012).

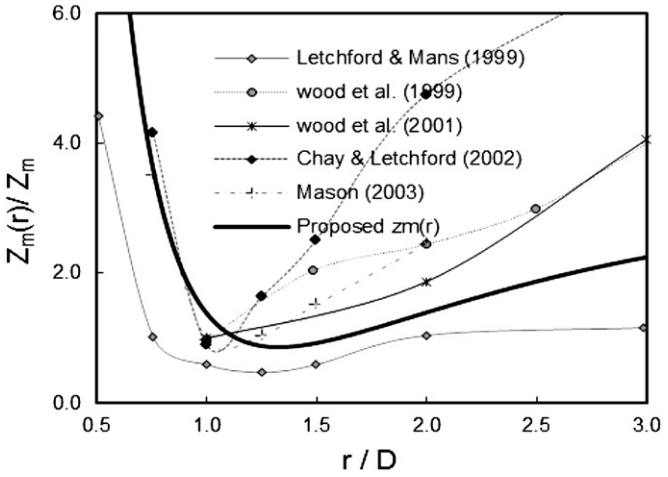


**Fig. 7.** Profile of $z_m$ along $r$.

However in this research, $z_m$ is used instead of $z^*$ to depict the effects of nonlinear growth of boundary layer thickness, whereas most structural systems are in the ranges of $z_m$ heights and the accurate description of wind profile at this altitude is more important. If $z_m(r)$ is identified as the height dependent radial of the maximum wind speed and $z_m$ is the location of the overall maximum horizontal speed in space, the relationship between $z_m(r)$ and $r/D$ can be established from the available numerical and experimental data given in Fig. 7 to have this form:

$$z_m(r) = z_m\left(\frac{1.1 + 7.0\left(\ln(r/D) - 0.2\right)^2}{(r/D)}\right) \tag{16}$$

### 4.2. Radial distance of maximum horizontal speed

Similar to changes of the height of maximum horizontal speed with radial distance, the radial coordinate of maximum horizontal speed changes with the height. Li et al. (2012) studied numerically the effect of boundary layer thickness on change of the radial coordinate of the maximum horizontal speed with elevation as shown in Fig. 8. They developed Eq. (17) to fit the profile of $r_m(z)$, where $r_m(z)$ is the radial dependent height of the maximum wind speed and the parameters $\eta$, $\iota$ and $\varphi$ are 2.01, 0.0078 and 0.0726, respectively. In the current study the parameter $\varphi$ has been

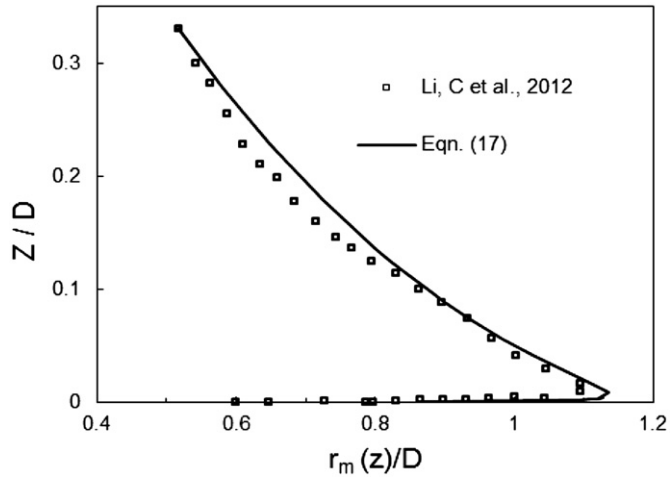


**Fig. 8.** Profile of $r_m(z)$ along $z$.

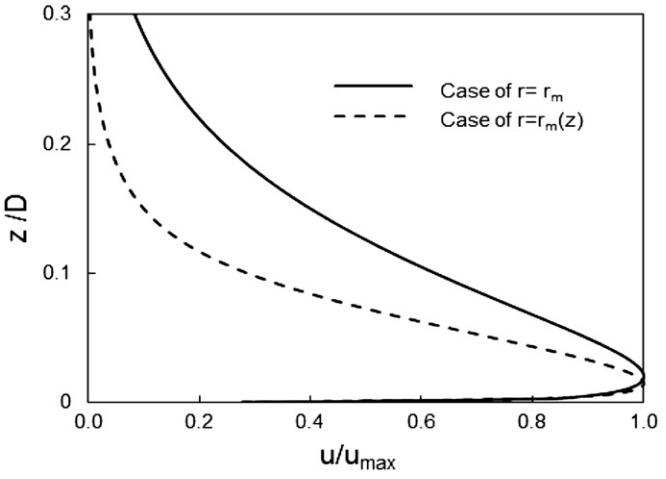


**Fig. 10.** Deviations in the shape of the vertical profile of horizontal speed due to replacing $r_m$ by $r_m(z)$.

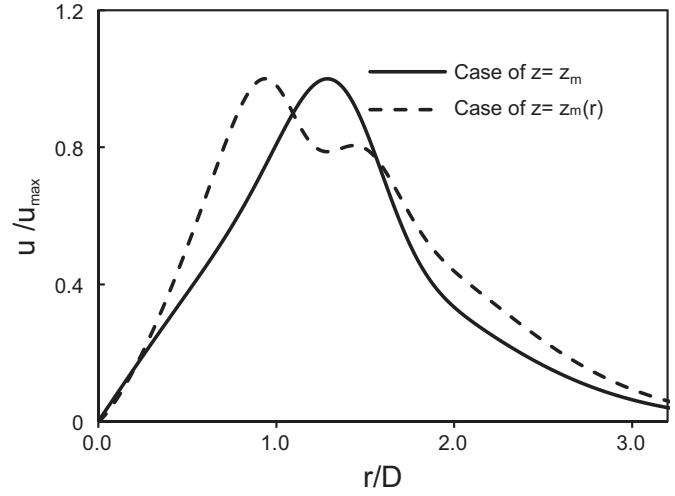


**Fig. 9.** Deviations in the shape of the radial profile of horizontal speed due to replacing $z_m$ by $z_m$ $(r)$.

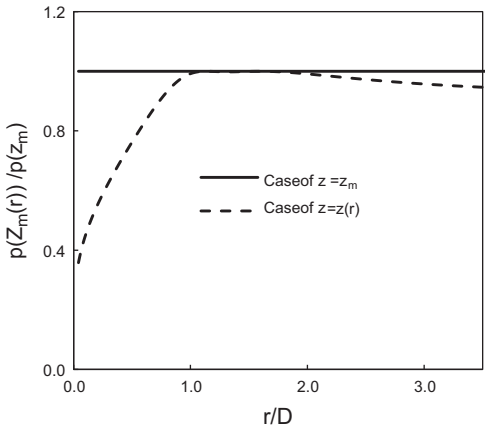


**Fig. 11.** Profile of normalised $(z)$ along.

improved to be 0.068 to give better fitting.

$$r_m(z) = \eta D - \frac{z}{l} e^{-\left(\frac{1-\left(\frac{z}{\eta D}\right)^{-\varphi}}{\varphi}\right)} \tag{17}$$

### 4.3. Incorporating the varied coordinates of the location of the maximum horizontal speed to the proposed model

Incorporating the varied vertical and radial coordinates of the location of the maximum horizontal velocity in Eqs. (16) and (17) into the previous model is not simple. If $z_m$ is replaced by $z_m(r)$ in the previous models, the vertical profiles of the speeds will be improved but the radial profiles will fail. The problem is similar if $r_m$ is replaced by $r_m$ $(z)$, the radial profiles of the speeds will be improved but the vertical profiles will be damaged, and if $z_m(r)$ and $r_m$ $(z)$ is utilized the two profiles radial and vertical of the speeds will be damaged. Figs. 9 and 10 explain the deviations in the shapes of the radial and the vertical profiles of horizontal wind speed due to incorporating the new radial and vertical coordinates of the maximum speed ($r_m$ $(z)$ and $z_m(r)$). The drops in the profiles result from the assumption in the original model of Oseguera and Bowles (1988) that the velocity is computed by multiplying two fixed profiles. The following example illustrates this problem.

The radial distribution of horizontal speed at defined height $z$ is computed by multiplying the two functions $f(r)$ and $p(z)$. At that defined height, the function $p(z)$ will have a constant value for all the radial coordinates while the function $f(r)$changes with the radial coordinate to depict the radial profile, then the total distribution for the speed is a scaled shape for $f(r)$ profile. However if $z_m$ is replaced by $z_m(r)$, the profile of the function $f(r)$ does not change, but the profile of the function $p(z)$ will change from a constant value to a nonlinear behavior (Fig. 11) and the total result is far from the required profile for the speed.

Researchers have rarely included the nonlinear growth of boundary layer thickness in the analytical models. Chay et al. (2006a) suggested replacing the height corresponding to maximum wind speed $z_m$ by the dependent height of maximum speed $z_m(r)$, but did not investigate this concept. Li et al. (2012) studied the inclusion of the effects of nonlinear growth of boundary layer thickness to the analytical models. They developed the three empirical (Eqs. (18)–(20)) to incorporate the boundary layer effects to the horizontal and vertical speed. The first equation is for depicting the vertical profile of the horizontal speed and is able to simulate the change of height of maximum speed $z_m(r)$ and the second equation is for depicting the radial profile of the horizontal speed and is able to simulate the change of dependent radial coordinate of maximum speed $r_m(z)$. The last equation is for deriving the vertical and the radial profiles of the vertical speed. They replaced the profile of $f(r)$ in Eq. (18) by profiles $u_{m,rs}(r)$ and the profile of $p(z)$ in Eq. (19) by the

profile $u_{m,vs}(z)$, where $u_{m,rs}(r)$and $u_{m,vs}(z)$ are the radial and vertical shaping functions of the maximum horizontal velocity, respectively.

$$u(z)|_r = u_{max} u_{m,rs}(r)\, p\left(\frac{z}{z_m(r)}\right) \tag{18}$$

$$u(r)|_z = u_{max} u_{m,vs}(z)\, f\left(\frac{r}{r_m(z)}\right) \tag{19}$$

$$w(r,z) = u_{max}\, g\left(\frac{r}{r_m(z)}^2\right) q\left(\frac{z}{z_m(r)}\right) \tag{20}$$

The Li et al. (2012) model has succeeded in incorporating the nonlinear effects of boundary layer thickness while simulating the horizontal speed, but failed to represent the profile of the vertical speed. The success in simulating the horizontal speed is due to separating the two dependent vertical and radial coordinates of maximum horizontal velocity $r_m(z)$ and $z_m(r)$ to two separated equations, but the drop in simulating vertical speed is due to incorporating the two dependent radial and vertical coordinates of the maximum speed $r_m(z)$ and $z_m(r)$ in one equation. This drop in simulating vertical speed is due to the alternative effect of the two dependent radial and vertical coordinates of the maximum horizontal velocity as discussed in the first part of this section. Furthermore, this model detached from the continuity equation which confirms the relation between the vertical and horizontal speed.

In this research, the previous model has been developed and the above-mentioned problems have been improved. The two functions $u_{m,rs}(r)$and $u_{m,vs}(z)$ have been replaced by the two functions $f_m(r)$ and $p_m(z)$, respectively, where these new two functions are able to depict the radial and vertical profile of the maximum horizontal speed (Figs. 12 and 13) and are given by the previous Eqs. (8) and (4) with different values for the parameters. Then Eqs. (18) and (19) will be similar to original model of Oseguera and Bowles (1988) (Eq. (A.3) in the Appendix) given by Eqs. (21) and (22), respectively. Each one of the two Eqs. (21) and (22) have been implemented separately to the continuity equation and the corresponding vertical velocity equations have been derived in Eqs. (23) and (24), respectively.

$$u(z)|_r = f_m(r)\, p\left(\frac{z}{z_m(r)}\right) \tag{21}$$

$$u(r)|_z = f\left(\frac{r}{r_m(z)}\right) p_m(z) \tag{22}$$

$$w(z)|_r = g_m(r^2)\, q\left(\frac{z}{z_m(r)}\right) \tag{23}$$

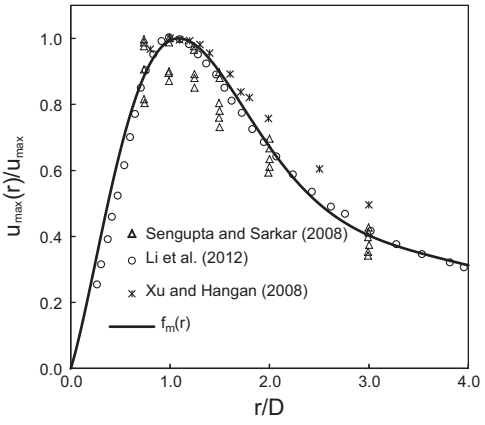


**Fig. 12.** Shaping function of $u_{max}(r)$.

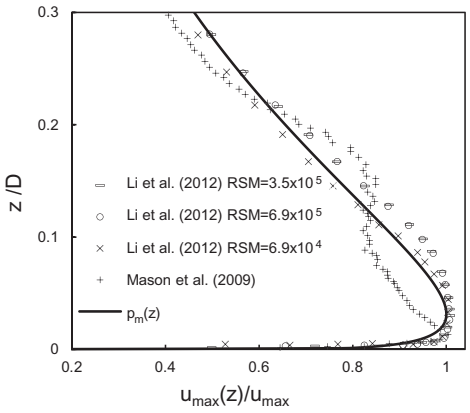


**Fig. 13.** Shaping function of $u_{max}(z)$.

$$w(r)|_z = g\left(\frac{r}{r_m(z)}^2\right) q_m(z) \tag{24}$$

By this technique, the nonlinear effects of boundary layer have been incorporated into the model without being detached from the continuity equation and the model becomes able to depict the profiles of horizontal speed and vertical speed. The model consists of two pairs of equations; the first pair consists of Eqs. (21) and (23) and the second pair consists of Eqs. (22) and (24) and each pair of equations is connected by the continuity equations. The first pair is for simulating the vertical profile of the horizontal and the vertical speeds, the second pair is for simulating the radial profile of the horizontal and the vertical speeds, and the two pairs are connected by the intensity parameter $\lambda$ (discussed in Section 4.4).

### 4.4. Model parameters

The new model consists of the four Eqs. (21)–(24). Since the Eqs. (23) and (24) have been derived from Eqs. (21) and (22), the parameters will therefore be calculated for the first two equations only. Eq. (21) consists of the two empirical functions $f_m(r)$ and $p(z/z_m(r))$ and Eq. (22) consists of the two empirical functions $p_m(z)$ and $f(r/r_m(z))$ and these functions will be calculated as below:

The function $f_m(r)$ is the shaping function of the maximum horizontal profile for the horizontal velocity. Several studies have estimated the radial profile of the maximum horizontal speed as shown in Fig. 12. Eq. (8) has been developed to fit the profile of maximum horizontal speed, but the authors preferred to use $r/D$ instead of $r/r_m$ to remove the interruption between $r_m$ and $r_m(z)$. The best fitting parameters for simulating the horizontal profile of the maximum horizontal speed are 2.0, 0.35, 0.18, 0.06 and 1.0 for the parameters $\delta,\gamma,\varepsilon,\kappa$ and $\chi$ respectively.

The function $p_m(z)$ is the shaping function of the maximum vertical profile of the horizontal velocity as shown in Fig. 13. Eq. (4) has been developed to fit the shaping profile of the maximum horizontal speed and $z/D$ has been used instead of $z/z_m$ to remove the interruption between $z_m$ and $z_m(r)$. The best fitting parameters to simulate the profile of the maximum horizontal speed are $-4.1$ and 1.1 for the parameters $c_1$ and $c_2$ respectively. The radial and vertical coordinates of the maximum speed $z_m(r)$ and $r_m(z)$ have been defined by Eqs. (16) and (17), respectively. $z_m$ and $r_m$ have been selected to be equal to $0.025D$ and $1.125D$, respectively, in agreement with Tables 1 and 2.

The functions $p(z/z_m(r))$ and $f(r/r_m(z))$are still defined by Eqs. (4) and (8) respectively, and their parameters will be discussed later. Then the final equations for the new model will

be in this form:

$$u(z)|_r = \frac{\lambda r}{2}\left[e^{-\left[0.7-(2r^2/D^2)^{0.35}\right]^2} + 0.18\, e^{-0.06(r^2/D^2)}\right] \left[\left(\frac{z}{z_m(r)}\right)^{c_2-1} x\, e^{c_1\left(\frac{z}{z_m(r)}\right)^{c_2}}\right] \quad (25)$$

$$u(r)|_z = \frac{\lambda r}{2}\left[e^{-\left[2\gamma-(\delta r^2/r_m(z)^2)^{\gamma}\right]^2} + \varepsilon e^{-\kappa(r^2/r_m(z)^2)^{\chi}}\right] \left[\left(\frac{z}{D}\right)^{0.1} x\, e^{c_1(\frac{z}{D})^{1.1}}\right] \quad (26)$$

And after implementing the two Eqs. (25) and (26) to continuity equations, the corresponding vertical velocity equations will be as shown in Eqs. (27) and (28).

$$w(z)|_r = -\lambda\left\{(1+0.7\psi(0.7-\psi))e^{-[0.7-\psi]^2} + 0.18\, e^{-0.06(r^2/D^2)} \left(1-\kappa\chi\left(\frac{r^2}{D^2}\right)\right)\right\} \times \left\{\frac{z_m(r)}{c_1 c_2}\left[e^{c_1\left(\frac{z}{z_m(r)}\right)^{c_2}}-1\right]\right\} \quad \text{and} \quad \psi = \left(\frac{2r^2}{D^2}\right)^{0.35} \quad (27)$$

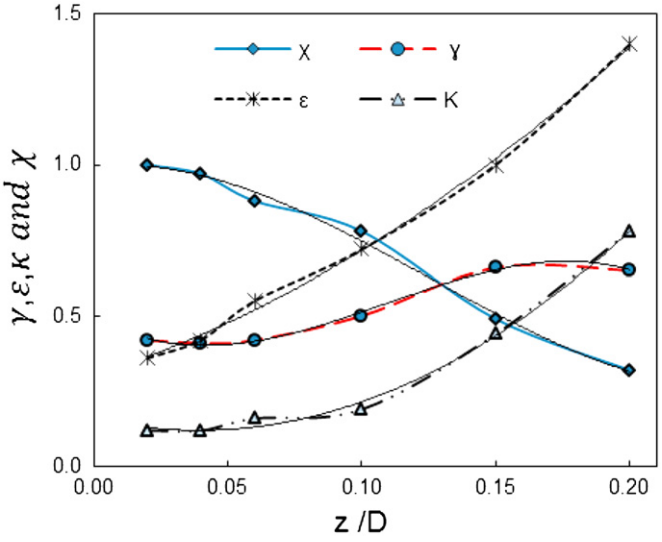


**Fig. 14.** Variations of the parameters $y$, $\varepsilon$, $\kappa$ and $\chi$ with $z/D$.

$$w(r)|_z = -\lambda\left\{(1+2\gamma\psi(2\gamma-\psi))e^{-[2\gamma-\psi]^2} + \varepsilon\, e^{-\kappa(r^2/r_z(m)^2)^{\chi}} \left(1-\kappa\chi\left(\frac{r^2}{r_z(m)^2}\right)^{\chi}\right)\right\} \times \left\{\frac{D}{-4.51}\left[e^{-4.1(\frac{z}{D})^{1.1}}-1\right]\right\} \quad \text{and} \quad \psi = \left(\frac{\delta r^2}{r_z(m)^2}\right)^{\gamma} \quad (28)$$

The new model now becomes able to depict the variations in the coordinates of maximum horizontal speed without being detached from the continuity equation.

The nonlinear effects of boundary layer thickness growth are not limited to the variation in the location of maximum horizontal speed only, the shapes of the profiles massively change along the vertical and the radial coordinates. The new Eq. (8) is characterized by its ability to depict the variation in the shapes of the wind profiles through developing relations between its parameters $\delta,\gamma,\varepsilon,\kappa$ and $\chi$ and the vertical coordinate. By investigation the variation in the profiles of horizontal speed with the elevation, the best values for the parameters at several heights are collected in Fig. 14 and simple polynomial relations between the parameters $\gamma,\varepsilon,\kappa$ and $\chi$ and vertical coordinates have been established in Eqs. (29) and (32). The parameter $\delta$ is still constant and equal to 2.1. The parameters of the vertical profile have been chosen for all coordinates as $c_1 = -0.16$ and $c_2 = 1/(1+c_1) = 1.19$.

$$\varepsilon = 12.938\,(z/D)^2 + 2.8563\,(z/D) + 0.3019 \quad (29)$$

$$\chi = 125.38\,(z/D)^3 - 46.849\,(z/D)^2 + 0.9688\,(z/D) + 0.9932 \quad (30)$$

$$\gamma = -227.69\,(z/D)^3 + 74.553\,(z/D)^2 - 5.0359\,(z/D) + 0.4985 \quad (31)$$

$$\kappa = 25.466\,(z/D)^2 - 1.9908\,(z/D) + 0.1593 \quad (32)$$

Using this proposed model, the maximum horizontal velocity can be expressed as Eq. (33) and the maximum vertical velocity at $r=0$ and $z=z_h$, is given by Eq. (34).

$$u_{max} = 0.338\,\lambda\, r_m \quad (33)$$

$$w_{max} = 1.919\,\lambda\, z_m\,(e^{c_1(z_h/z_m)^{c_2}}-1) \;\; and \;\; c_1 = -0.16 \;\; and \;\; c_2 = 1.19 \quad (34)$$

The scaling factor $\lambda$ can be determined by using either Eq. (33) or (34) and setting it equal to $u_{max}$ or $w_{max}$, respectively.

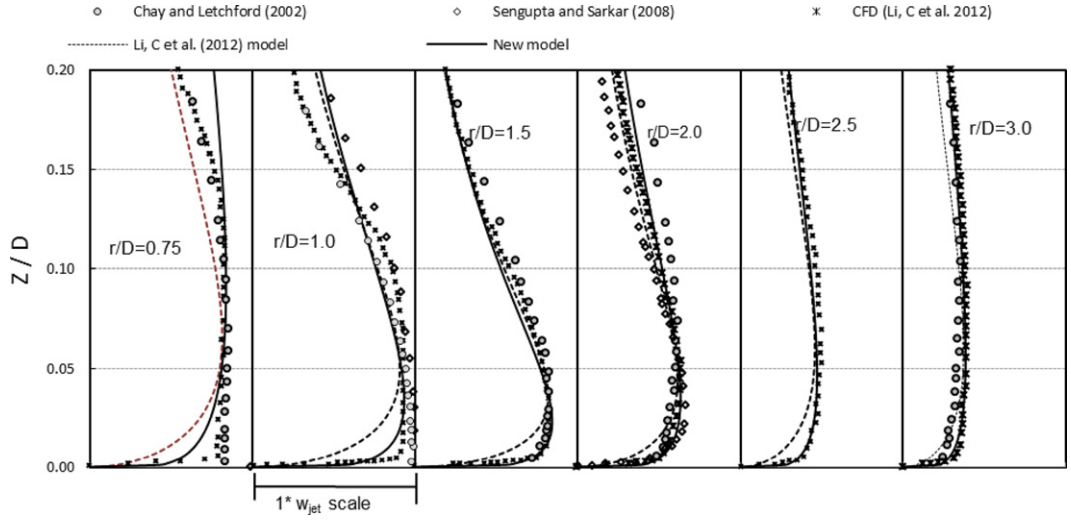


**Fig. 15.** Vertical profiles of horizontal velocity.

### 4.5. Model verification

The model has been validated by comparing its results with the results from several numerical and experimental studies (Chay and Letchford, 2002; Sengupta and Sarkar, 2008; Xu and Hangan, 2008; Li et al., 2012). Chay and Letchford (2002) studied the profiles of downburst wind using a stationary wall jet tunnel. They stated that the wall jets displayed similar 'mean' velocity characteristics to reported full-scale downbursts, especially, the variation of speed with height above the ground. Xu and Hangan (2008) studied experimentally the simulation of downburst wind profiles. They investigated the axial orthonormal impinging jet flow and the cloud-base height, scale, boundary conditions and terrain roughness that have been encountered in downburst simulations. Sengupta and Sarkar (2008) investigated experimentally and numerically the downburst wind profiles, by simulating the downburst using a round jet impinging onto a flat plate. Their experimental data was collected using hotwire, particle image velocimetry (PIV) and pressure rakes. They confirmed a favourable agreement between the numerical and the experimental results. Li et al. (2012) investigated downburst wind speed numerically. They utilized a 3D computational domain using Cartesian coordinate system. The impinging jet flow and downbursts have been regarded as incompressible and solved using finite volume methods (FVM).

The velocity field of the new model has been calculated directly by using Eqs. (25) and (27) for the vertical distribution of the horizontal and the vertical speed, and Eqs. (26) and (28) have been used for calculating the radial distribution of the horizontal and the vertical speed, respectively. By substituting $z_m(r)$ and $r_m(z)$ from Eqs. (16) and (17) respectively, and the model parameters discussed in Section 4.4, the vertical profile of the horizontal and vertical speeds at distances $r/D=0.75$, 1.0, 1.5, 2.0, 2.5 and 3.0 are plotted in Figs. 15 and 16, respectively.

The new model simulated the vertical profile of horizontal speed with higher accuracy than the previous models, in particular, at short heights ($z/D<0.05$). Hjelmfelt (1988) showed that the downdraft diameter ranged from 1.5 to 3.0 km and through this range most structural systems are at this short height of less than 75–150 m. Added to that, the model succeeded in simulating the vertical profile of the vertical speed. The radial profiles of the horizontal and vertical speeds at $z/D=0.02$, 0.04, 0.06, 0.1, 0.15 and 0.2 are plotted in Figs. 17 and 18, respectively. The new model significantly matches CFD results and is characterized by its ability to change and depict shapes of the radial profile of the horizontal speed at each height while achieving radial and vertical coordinates of the location of the maximum horizontal

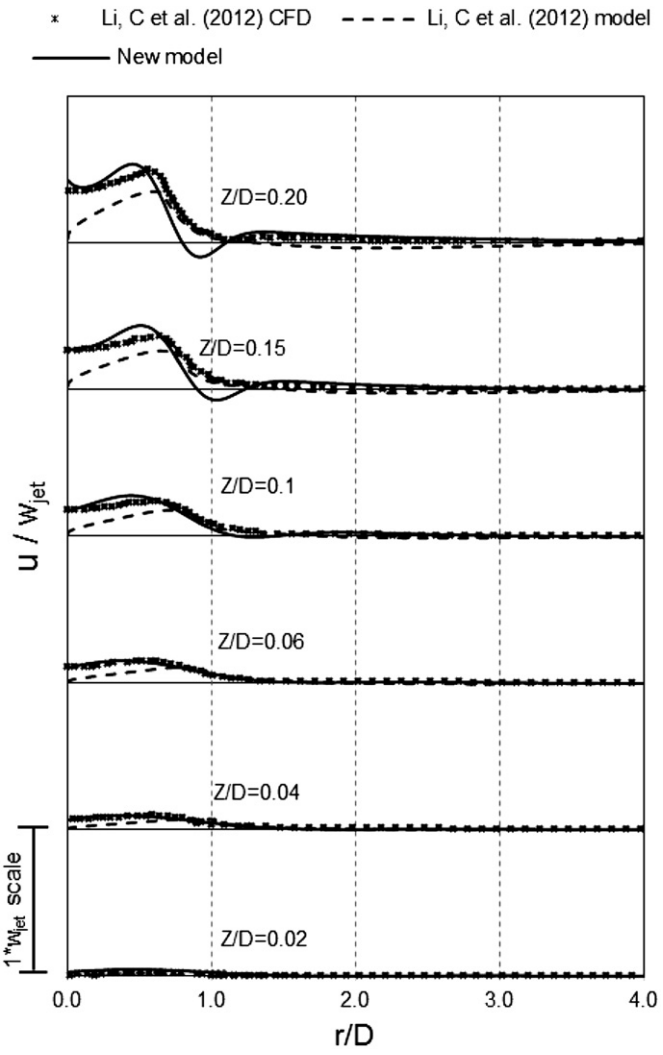


**Fig. 17.** Radial profiles of horizontal velocity.

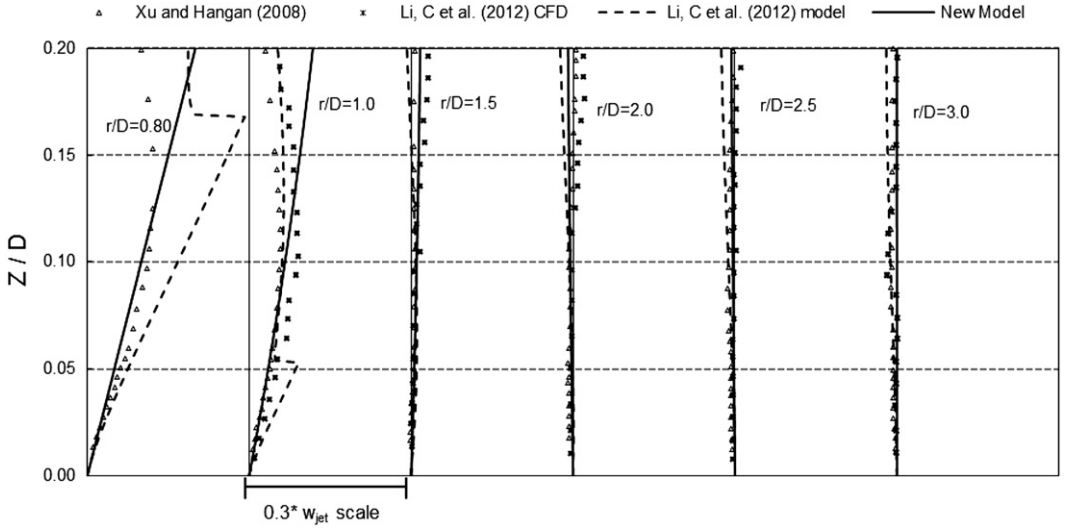


**Fig. 16.** Vertical profiles of horizontal velocity.

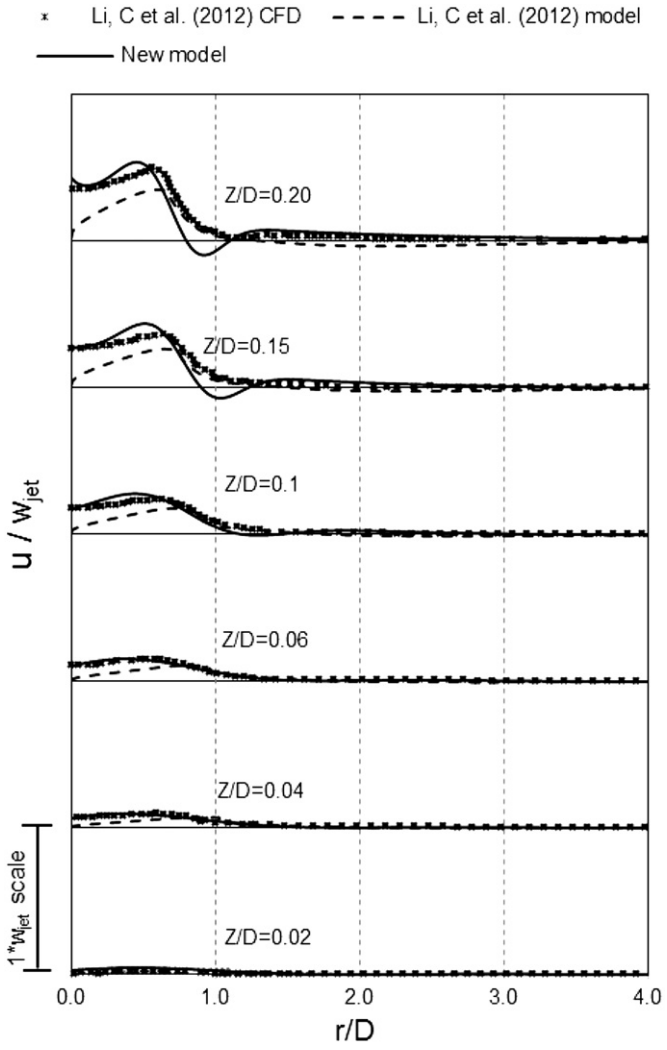


**Fig. 18.** Radial profiles of vertical velocity.

speed. Furthermore, it succeeded in depicting the radial profile of the vertical speed.

## 5. Conclusion

Several analytical models have been developed for simulating downburst models, but there are disparities between the profiles of these models and the actual profiles. In addition, the effects of the nonlinear growth of boundary layer thickness are rarely included. A new analytical model based on the collection of numerical, experimental simulation results and recorded field data with the mass continuity equation has been developed. Several improvements have been presented including:

- A new pair of shaping functions which are more accurate for simulating the profiles of horizontal wind speed and match the available field and numerical data have been developed. The new shaping function for the vertical profile is characterized by having a simple integration that simplifies the model and makes the model more useful for practical situations. The new shaping function for the radial profile has the ability to modify their profiles with the altitude.
- The vertical and radial profiles of vertical speeds have been derived from the vertical and radial profiles of horizontal speeds by using the Euler and mass continuity equations that strengthen the relationship between the vertical and the horizontal speed since the relationship depends on physical basis.
- The proposed model is able to depict the primary changes in shapes of the profiles of speed due to the effects of nonlinear growth of boundary layer thickness. It compares well with most recent models in the range of "$r<3D$ and $z<0.2D$" and it enhances the depiction of coordinates of maximum horizontal speed.
- Compared with the model of Li et al. (2012), the proposed model succeeded in incorporating the nonlinear effects to the horizontal and the vertical velocities with realizing the continuity equation. In addition the new model achieves simplicity with higher accuracy than the previous models.

The new model simulates the velocity field for steady state flows of downburst but there is a need for multiplying this model by a developed time function to be able to simulate the unsteady state flows of downburst. This is the aim of future work to be undertaken by the authors.

## Appendix

Oseguera and Bowles (1988), Vicroy (1991) and Vicroy (1992) developed an analytical model for simulating downburst wind loads by solving the mass continuity equation and assuming a pair of shaping functions that were able to simulate velocity profiles matching TASS. These models are summarized here.

The mass continuity equation for steady state flow in cylindrical coordinates is:

$$\frac{\partial \rho}{\partial t}+\frac{1}{r}\frac{\partial}{\partial r}(\rho r u)+\frac{1}{r}\frac{\partial(\rho v)}{\partial \phi}+\frac{\partial(\rho w)}{\partial z}=0 \tag{A.1}$$

With the assumption of no tangential velocity ($v=0$), the remaining quantities are independent of $\phi$, assuming the flow is incompressible then $\rho$ is constant and the continuity equation is reduced to:

$$\frac{\partial u}{\partial r}+\frac{\partial w}{\partial z}+\frac{u}{r}=0 \tag{A.2}$$

This equation can be solved by the form:

$$u=f(r)\,p(z) \tag{A.3}$$

$$w=g(r^2)\,q(z) \tag{A.4}$$

Provided that

$$\frac{\partial q(z)}{\partial z}=-\lambda p(z) \tag{A.5}$$

$$\frac{\partial[rf(r)]}{\partial r^2}=\frac{\lambda}{2}\,g(r^2) \tag{A.6}$$

where $f(r)$ is the radial shaping function of the horizontal wind velocity; $g(r^2)$is the radial shaping function of the vertical wind velocity; $p(z)$ is the vertical shaping function of the horizontal wind velocity; $q(z)$ is the vertical shaping function of the vertical wind velocity; $\lambda$ is the scaling factor.

The selected shaping function for the vertical and the radial profile of the horizontal wind speed that were used in the models of Vicroy (1991 and 1992) are given by Eqs. (A.7) and (A.8), respectively:

$$p(z)=e^{\xi_1(z/z_m)}-e^{\xi_2(z/z_m)} \tag{A.7}$$

$$f(r)=\frac{\lambda r}{2}e^{\left[\frac{1-\left(r^2/\beta^2\right)^{\alpha}}{\alpha}\right]} \tag{A.8}$$

where $\xi_1$, $\xi_2$,$\alpha$ and $\beta$ are shaping function variables.

The vertical and the radial shaping functions of the vertical wind speed $q(z)$ and $g(r^2)$ have been derived from Eqs. (A.5) and (A.6), respectively as:

$$q(z)=-\lambda\left\{\frac{z_m}{\xi_1}\left[e^{\xi_1\left(\frac{z}{z_m}\right)}-1\right]-\frac{z_m}{\xi_2}\left[e^{\xi_2\left(\frac{z}{z_m}\right)}-1\right]\right\} \tag{A.9}$$

$$g\left(r^2\right)=\left[1-\left(\frac{r^2}{\beta^2}\right)^{\alpha}\right]e^{\left[\frac{1-\left(r^2/\beta^2\right)^{\alpha}}{\alpha}\right]} \tag{A.10}$$

Combining the shaping functions as in Eqs. (A.3) and (A.4), the horizontal and vertical wind speeds are expressed as follows:

$$u=\frac{\lambda r}{2}\left[e^{\xi_1\left(\frac{z}{z_m}\right)}-e^{\xi_2\left(\frac{z}{z_m}\right)}\right]e^{\left[\frac{1-\left(r^2/\beta^2\right)^{\alpha}}{\alpha}\right]} \tag{A.11}$$

$$w=\left\{\frac{z_m}{\xi_1}\left[e^{\xi_1\left(\frac{z}{z_m}\right)}-1\right]-\frac{z_m}{\xi_2}\left[e^{\xi_2\left(\frac{z}{z_m}\right)}-1\right]\right\}\left[1-\left(\frac{r^2}{\beta^2}\right)^{\alpha}\right]e^{\left[\frac{1-\left(r^2/\beta^2\right)^{\alpha}}{\alpha}\right]} \tag{A.12}$$

## References


Chay, M.T., Albermani, F., Wilson, R., 2006a. Numerical and analytical simulation of downburst wind loads. Engineering Structures 28 (2), 240–254.

Chay, M.T., Albermani, F., Hawes. H, 2006b. Wind loads on transmission line structures in simulated downbursts. In: Conference, First World Congress on Asset Management.

Chay, M.T., Letchford, C.W., 2002. Pressure distributions on a cube in a simulated thunderstorm downburst-Part A: stationary downburts observations. Journal of wind engineering and industrial aerodynamics 90 (7), 711.

Dempsey, D., White, H.B., 1996. Winds wreak havoc on lines. Transmission and Distribution World 48(6), 32–42.

'Downbursts' of air are called danger to aircraft, 1979. The Globe and Mail, 21.

Hangan, H., Roberts, D., Xu, Z., Kim, J., 2003. Downburst simulation, experimental and numerical challenges. In: Proceedings of the 11th International Conference on Wind Engineering, Lubbock, TX, Electronic Version.

Hjelmfelt, M.R., 1988. Structure and life cycle of microburst outflows observed in Colorado. Journal of Applied Meteorology 27 (8), 900–927.

Holmes, J.D., Oliver, S.E., 2000. An empirical model of a downburst. Engineering Structures 22 (9), 1167–1172.

Kim, J., Hangan, H., 2007. Numerical simulations of impinging jets with application to downbursts. Journal of Wind Engineering and Industrial Aerodynamics 95 (4), 279–298.

Letchford, C.W., Mans, C., 1999. Physical Modeling of Thunderstorm Downbursts by a Moving Wall Jet. University of Queensland, for Powerlink, Brisbane, Queensland, Australia.

Li, C., Li, Q.S., Xiao, Y.Q., Ou, J.P., 2012. A revised empirical model and CFD simulations for 3D axisymmetric steady-state flows of downbursts and impinging jets. Journal of Wind Engineering and Industrial Aerodynamics 102, 48–60.

Li, C.Q., 2000. A stochastic model of severe thunderstorms for transmission line design. Probabilistic Engineering Mechanics 15 (4), 359–364.

Mason, M.S., 2003. Pulsed Jet Simulation of Thunderstorm Downbursts. Master Thesis. Texas Tech University.

Mason, M.S., Wood, G.S., Fletcher, D.F., 2009. Numerical simulation of downburst winds. Journal of Wind Engineering and Industrial Aerodynamics 97 (11–12), 523–539.

McCarthy, P. Melsness, M. 1996. Severe weather elements associated with September 5, 1996 hydro tower failures near Grosse Isle, Manitoba, Canada. Manitoba Environmental Service Centre, Environment Canada. , 21pp.

McConville, A.C., Sterling, M., Baker, C.J., 2009. The physical simulation of thunderstorm downbursts using an impinging jet. Wind and Structures 12 (11), 133–149.

Oseguera, R., Bowles, R., 1988. A simple, analytic 3-dimensional downburst model based on boundary layer stagnation flow. NASA Technical Memorandum, 100632.

Proctor, F. H., 1987. The Terminal Area Simulation System. Volume II: Verification Cases. NASA CR-4046, April 1987.

Sengupta, A., Sarkar, P.P., 2008. Experimental measurement and numerical simulation of an impinging jet with application to thunderstorm microburst winds. Journal of Wind Engineering and Industrial Aerodynamics 96 (3), 345–365.

Shehata, A.Y., Nassef, A.O., El Damatty, A.A., 2008. A coupled finite element-optimization technique to determine critical microburst parameters for transmission towers. Finite Elements in Analysis and Design 45 (1), 1–12.

Vermeire, B.C., Orf, L.G., Savory, E., 2011. Improved modelling of downburst outflows for wind engineering applications using a cooling source approach. Journal of Wind Engineering and Industrial Aerodynamics 99 (8), 801–814.

Vicroy, D., 1991. A simple, analytical, axisymmetric microburst model for downdraft estimation. NASA Technical Memorandum, 104053. Vicroy, D., 1992. Assessment of microburst models for downdraft estimation. Journal of Aircraft 29 (6), 1043–1048.

Vicroy, D., 1992. Assessment of microburst models for downdraft estimation. Journal of Aircraft 29 (6), 1043–1048.

Wood, G.S., Kwok, K.C., Motteram, N.A., Fletcher, D.F., 2001. Physical and numerical modelling of thunderstorm downbursts. Journal of Wind Engineering and Industrial Aerodynamics 89 (6), 535–552.

Wood, G.S., Kwok, K.C., Motteram, N.A., Fletcher, D.F., 1999. Physical and numerical modelling of thunderstorm downbursts. In: Wind Engineering into the 21st Century: Proceedings of the 10th International Conference on Wind Engineering 3. pp. 1919–1924.

Xu, Z., Hangan, H., 2008. Scale, boundary and inlet condition effects on impinging jets. Journal of Wind Engineering and Industrial Aerodynamics 96 (12), 2383–2402.

Zhang, Y., 2006. Status quo of wind hazard prevention for transmission lines and countermeasures. East China Electric Power 34 (3), 28–31.